This article was downloaded by:
On: *14 January 2011*
Access details: *Access Details: Free Access*
Publisher *Taylor & Francis*
Informa Ltd Registered in England and Wales Registered Number: 1072954 Registered office: Mortimer House, 37-41 Mortimer Street, London W1T 3JH, UK

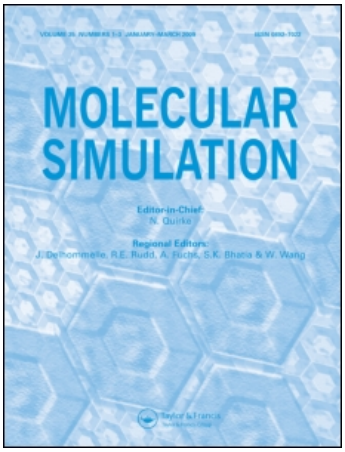

Molecular Simulation
Publication details, including instructions for authors and subscription information:
http://www.informaworld.com/smpp/title~content=t713644482

Lattice kinetic Monte Carlo simulations of defect evolution in crystals at elevated temperature

J. Dai[a]; W. D. Seider[a]; T. Sinno[a]
[a] Department of Chemical and Biomolecular Engineering, University of Pennsylvania, Philadelphia, PA, USA

To cite this Article Dai, J. , Seider, W. D. and Sinno, T.(2006) 'Lattice kinetic Monte Carlo simulations of defect evolution in crystals at elevated temperature', Molecular Simulation, 32: 3, 305 — 314
To link to this Article: DOI: 10.1080/08927020600586557
URL: http://dx.doi.org/10.1080/08927020600586557

PLEASE SCROLL DOWN FOR ARTICLE

Full terms and conditions of use: http://www.informaworld.com/terms-and-conditions-of-access.pdf

This article may be used for research, teaching and private study purposes. Any substantial or systematic reproduction, re-distribution, re-selling, loan or sub-licensing, systematic supply or distribution in any form to anyone is expressly forbidden.

The publisher does not give any warranty express or implied or make any representation that the contents will be complete or accurate or up to date. The accuracy of any instructions, formulae and drug doses should be independently verified with primary sources. The publisher shall not be liable for any loss, actions, claims, proceedings, demand or costs or damages whatsoever or howsoever caused arising directly or indirectly in connection with or arising out of the use of this material.

Molecular Simulation, Vol. 32, Nos. 3–4, 15 March–April 2006, 305–314

Taylor & Francis
Taylor & Francis Group

Lattice kinetic Monte Carlo simulations of defect evolution in crystals at elevated temperature

J. DAI, W. D. SEIDER and T. SINNO*

Department of Chemical and Biomolecular Engineering, University of Pennsylvania, Philadelphia, PA 19104, USA

(Received December 2005; in final form January 2006)

A lattice kinetic Monte Carlo (LKMC) model for vacancy diffusion and aggregation in crystalline silicon at elevated temperature is developed and analyzed in detail by comparing predicted cluster aggregation, thermodynamics, structures and diffusivities with properties obtained from molecular dynamics (MD) simulations. The lattice KMC model is based on a long-range bond-counting scheme in which the bond energies are determined by regression to a single non-equilibrium MD simulation of vacancy aggregation. It is shown that the resulting KMC model is able to capture important high temperature entropic contributions by coarse-graining off-lattice relaxations around defect clusters.

Keywords: Lattice kinetic Monte Carlo; Silicon; Vacancy aggregation; Configurational entropy

Downloaded At: 18:13 14 January 2011

1. Introduction

The kinetic Monte Carlo (KMC) method is ideally suited for the simulation of atomic diffusion and aggregation in crystalline materials such as semiconductors and metals. KMC essentially coarse-grains the details of atomic vibration that severely limit the scope of molecular dynamics (MD) simulations while retaining atomistic resolution. In crystalline systems, the presence of a lattice naturally suggests the application of on-lattice KMC (LKMC), which can be a particularly efficient variant of KMC [1,2]. In LKMC, the domain is discretized onto a fixed lattice on which mobile particles can hop and interact. The increased efficiency of LKMC relative to continuous space implementations arises from reductions in the available spatial degrees of freedom and in the number of different possible processes that can occur at any one time.

The principal drawback of LKMC is that mechanistic and rate information must be supplied externally [3]. This is in contrast to MD simulation that only requires the specification of an interatomic force field. The required inputs for LKMC simulations are rates for the various allowable events, typically diffusion, reaction and clustering. There are several approaches for specifying the rate process database in a LKMC simulation [4–8]. These include: (1) full enumeration of all possible transitions; (2) specifying a fixed set of possible events; (3) using the change in the number of bonds between species on neighboring lattice sites that result from a transition; and (4) "on-the-fly" using a potential energy function to find barriers out of a given configuration. The rates for the different possible events are usually calculated within the context of transition-state theory (TST) [9,10]. In this approach, the rate of a particular transition is computed by identifying the dividing surface in the potential energy landscape between an initial and a final state and then analyzing the crossings across this surface. Additional approximations within the framework of TST can be made to further simplify the evaluation of rates. The most common of these is the harmonic approximation in which the overall rate is decomposed into a temperature independent energy barrier and a preexponential factor. The latter can be computed using a harmonic normal mode analysis at the initial and saddle point configurations [11,12] but is often assumed to be a single constant for all processes during a simulation.

The KMC method (lattice or otherwise) is particularly attractive at low temperatures where thermally activated processes are slow and therefore each particle move represents a long time increment. For example, KMC simulations of atomic diffusion and aggregation on metallic surfaces can span times of seconds and longer at temperatures below 300 K [13]. Under these conditions,

*Corresponding author. Email: talid@seas.upenn.edu

Molecular Simulation
ISSN 0892-7022 print/ISSN 1029-0435 online © 2006 Taylor & Francis
http://www.tandf.co.uk/journals
DOI: 10.1080/08927020600586557

the underlying picture that the diffusion and aggregation proceed as a sequence of uncorrelated rare-events that take place on lattice sites also becomes more accurate. Moreover, MD simulation is extremely inefficient at low temperatures making alternative simulation approaches necessary for studying dynamical phenomena.

On the other hand, much of the processing of crystalline semiconductors and metals occurs at elevated temperature. While KMC becomes less efficient at higher temperatures, it is still a valuable tool that allows for a much broader atomistic picture than any MD simulation. In this paper, we analyze in detail a lattice KMC model for vacancy aggregation in crystalline silicon at elevated temperature. Vacancy aggregation in silicon is a valuable prototypical model for solid-state diffusion, nucleation and growth because it is commercially important and has been studied extensively with experiments [14,15] and continuum models [16–18], offering many opportunities for model validation. Finally, several accurate empirical interatomic potentials are readily available for modeling defect evolution in silicon [19–21].

High temperature vacancy aggregation in silicon is characterized by several features that make lattice KMC modeling challenging. The first is that vacancy–vacancy interactions are relatively long-ranged, extending up to the 8th neighbor shell [22,23]. This feature greatly increases the number of different processes that can exist and necessitates the formulation of a compact model for describing all the possibilities. A second characteristic of the vacancy-in-silicon system that is especially important to consider in the context of LKMC simulation is its quasi-continuous nature. Here, the term *quasi-continuous* is used to describe the fact that although the system is coarsely characterized by the tetrahedral silicon lattice, vacancy cluster configurations at high temperature become increasingly characterized by off-lattice relaxations. These relaxations lead to significant effects on both the kinetics and thermodynamics of the aggregation process and must somehow be accounted for.

In a previous paper [24], we presented a methodology for using data generated by a single non-equilibrium MD simulation to tune, using regression, a KMC bonding model for vacancy aggregation at high temperature. We demonstrated how various features of the bonding model, such as interaction range and shielding, are required to capture quantitatively the evolution dynamics. In the present work, we analyze this MD-regressed KMC model in detail by comparing its predictions for various cluster properties, such as diffusivities, structures and formation thermodynamics, to values obtained from independent MD simulations. We also analyze a related LKMC model parameterized entirely using lattice structures.

2. Lattice KMC model for vacancy aggregation

The details of the LKMC algorithm employed in this work have been presented elsewhere [24] and here we provide only a brief summary. The simulation system is initialized by placing a number of vacancies onto a cubic lattice subject to periodic boundaries. A matrix containing the rates for all possible hops from the initial configuration is initialized. The individual rates are grouped into event types according to value and a standard binary-tree search algorithm is used to pick an event type based on its total contribution to the overall rate. Once an event type is selected, a particular particle is randomly chosen to execute the event (from the appropriate subset of particles). Once the selected event is executed, the local configuration and the rate database for vacancies that are within interaction range of the hopping vacancy are updated. After each event, the simulation time is updated using $\Delta t = -(\ln U)/P$, where U is a uniform random number, $U \in [0,1]$ and P is the current sum of all possible rates. The algorithm is repeated until the required time is reached.

A bond-counting approach is used to specify the rates of each possible vacancy hop. The model is a generalization of the model developed by La Magna *et al.* [25] and now includes interactions up to the 8th nearest-neighbor (8NN) distance [24]. An important feature of this model was the inclusion of a "screening" effect that effectively shields some of the vacancy–vacancy interactions. For example, 2nd nearest neighbor (2NN) interactions were shielded (i.e. deactivated) if the shared 1st nearest-neighbor (1NN) site was occupied by a vacancy. The addition of bond-screening changes the overall cluster energy scaling and accounts for the fact that the energy of formation for a cavity arises solely from the dangling bonds of lattice atoms at its surface [26]—the vacancy–vacancy "bond" is simply a convenient construct that allows mapping of the overall system onto the vacancy positions.

Examples of vacancy–vacancy bonds for a variety of configurations are shown in figure 1. For any given vacancy pair within interaction distance, the interaction is screened if there exist one or more vacancies that are

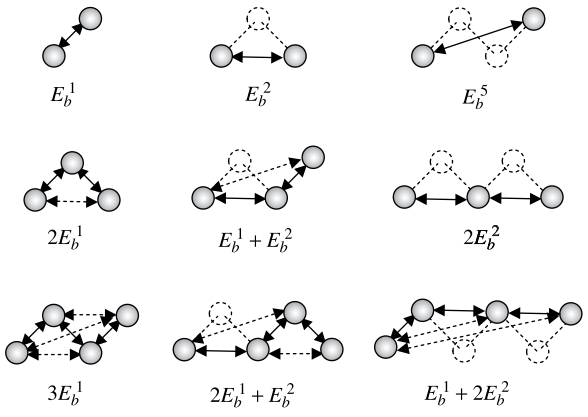

Figure 1. Examples of bonding for various cluster configurations aligned along the (110) crystallographic direction. First row: dimer configurations, second row: trimer configurations, third row: tetramer configurations. Shaded spheres represent vacancies, empty spheres represent lattice atoms. Solid lines indicate active interactions, dashed lines indicate screened interactions. Note that only atoms along a single (110) direction are shown.

Downloaded At: 18:13 14 January 2011

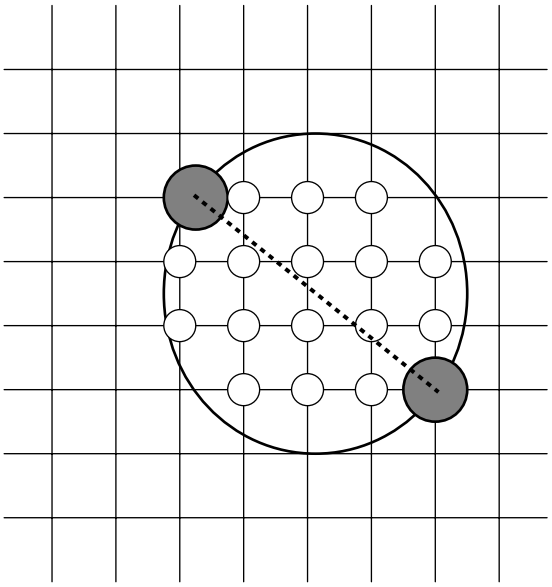

Figure 2. Two-dimensional representation of screening volume between two vacancies (gray circles). Any occupied lattice sites (small white circles) within large circle lead to screening of the interaction between the two vacancies.

Downloaded At: 18:13 14 January 2011

closer to both than they are to each other. The screening volume around two particles is determined by constructing a sphere so that the particles lie on its circumference and are connected by a diameter as shown schematically in figure 2. The interaction between the two vacancies shown is screened if there are one or more vacancies in the sphere.

2.1 Rate estimation framework

Energy barriers for all possible vacancy hops are computed using an approximate compact formulation within the TST framework given by [27]

$$\Delta E_{\text{total}} = 0.5 \times (E_{\text{final}} - E_{\text{init}}) + \Delta E_{\text{hop}}. \tag{1}$$

where E_{final} and E_{init} are the energies of the configurations after and before a given hop, respectively, and ΔE_{hop} is the energy barrier for a single, isolated vacancy jump. The energy barrier for any transition can be expressed explicitly in terms of the vacancy–vacancy bond energies by

$$\Delta E_i = \max\left(0,\ \Delta E_{\text{hop}} - 0.5 \times \sum_{j=1}^{\text{NN}} \left[\Delta \text{NB}_j E_b^j\right]\right), \tag{2}$$

where ΔE_i is the energy barrier for event i, NN is the maximum interaction shell, ΔNB_j is the bond count change due to a hop associated with interaction range j and E_b^j is the corresponding bond energy. Note that all barriers are positive; if the energy difference between the initial and final states is negative and larger in magnitude than ΔE_{hop}, no energy barrier exists for the hop. The rate of an event i is then simply given by an Arrhenius expression of the form

$$r_i = \nu_0 \exp\left(\frac{-\Delta E_i}{k_B T}\right) \tag{3}$$

where r_i is the rate for event i, ν_0 is a system-wide attempt frequency, k_B is the Boltzmann constant and T is the simulation temperature.

3. Results and discussion

The vacancy–vacancy bond energies were determined using two different approaches that will be discussed separately in the following sections. In both cases, the basic elements of the KMC model described above are the same—the only difference is in how the bond energies in equation (2) are computed. In the first case, which we denote as the lattice-cluster KMC model, the bond energies are determined by considering various on-lattice cluster structures. In the second approach, leading to the MD-regressed KMC model, the bond energies are determined by regression of the KMC evolution profiles to MD generated data. The performance of both models was investigated by comparison to non-equilibrium large-scale MD simulations.

3.1 Lattice-cluster KMC model

Here, a fully on-lattice picture is used in which the bond energies are obtained by considering an ensemble of on-lattice configurations for some selected cluster sizes. On-lattice connected configurations (i.e. every vacancy was within the 8NN shell of at least one other vacancy) were generated randomly. Each configuration first was relaxed with conjugate gradient energy minimization (based on the environment dependent interatomic potential (EDIP) for silicon [19]) and then its formation energy was computed by reference to a perfect crystal system containing the same number of atoms [28]. The energy minimization procedure captures the potential energy surface predicted by the EDIP potential in the neighborhood of each on-lattice configuration. About 60,000 configurations were generated and relaxed. This data was then used to regress the eight bond energies $\{E_b^1, E_b^2, \ldots, E_b^8\}$ according to the relationship

$$E_f(n) = 3.23n - \sum_n \sum_{i=1}^{\text{NN}} \left[\text{NB}_i E_b^i\right], \tag{4}$$

where NB_i is the number of vacancy–vacancy bonds of type i associated with n vacancies. The first term in equation (4) represents the formation energy for n single isolated vacancies.

As shown in figure 3, the bond-energy model is able to reproduce almost exactly the formation energy of all configurations for several different cluster sizes ranging from 6 to 18. Note that screening physics discussed earlier were taken into account during bond energy regression.

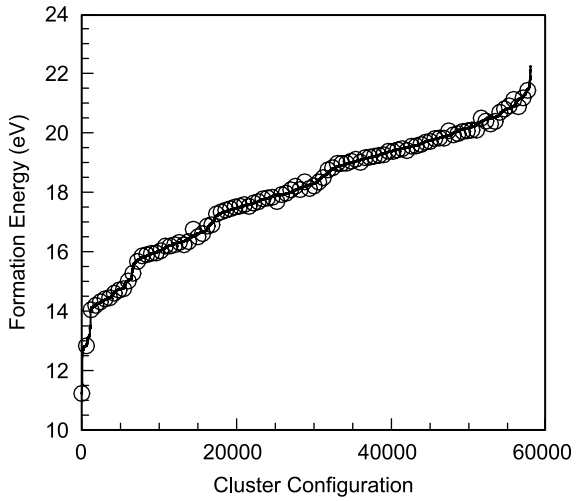

Figure 3. Formation energies for approx. 60,000 relaxed on-lattice configurations for several different cluster sizes ranging from 6 to 18 computed with: (a) energy minimization (solid line); and (b) KMC bond model fit (circles). Configurations are sorted in order of increasing formation energy. Note that only a small fraction of the KMC bond model fit data is shown for clarity.

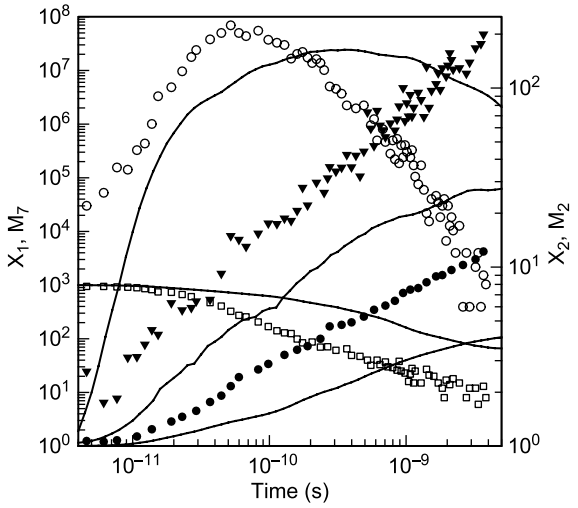

Figure 4. Comparison of MD and lattice-cluster KMC model predictions for the vacancy cluster size evolution. Evolution profiles are symbols for MD, solid line for KMC: X_1—monomer (open squares); X_2—dimer (open circles); M_2—average cluster size (solid circles); M_7—seventh-order moment (solid gradients).

Downloaded At: 18:13 14 January 2011

The attempt frequency, ν_0, in equation (3) and the single isolated vacancy migration barrier, ΔE_{hop}, were determined on the basis of MD simulation of single vacancy diffusion at 1600 K. These values were taken to be $9.5 \times 10^{13}\,\text{s}^{-1}$ and 0.3 eV, respectively.

The validity of the lattice-cluster KMC model was evaluated by direct comparison to MD predictions for the following non-equilibrium simulation: A total of 1000 equidistant single vacancies were introduced into a periodic cubic silicon crystal containing 216,000 lattice sites at 1600 K and zero pressure. The NVT ensemble MD simulations were performed using the empirical EDIP potential [19]. Velocity rescaling [29] was used for temperature control and the system was propagated with the Gear 5th order predictor–corrector algorithm. The highly super-saturated system was allowed to evolve for about 4 ns, corresponding to about 5×10^6 time steps. The vacancy cluster size distribution was periodically computed using the approach described in Ref. [23].

A comparison between the lattice-cluster KMC model and MD results for several components of the vacancy cluster size distribution is shown in figure 4. Both individual components (monomer (X_1) and dimer (X_2) numbers) as well as moment measures are used in the comparison. Moments of the size distribution are defined as $M_n = \sum_s s^n X_s$, where X_s is the number of clusters of size s and n is the moment order. The lattice-cluster KMC model clearly under-predicts the aggregation dynamics. The bond energies in the lattice-cluster KMC model are such that clusters of all sizes are predicted to be tightly bound and therefore almost immobile. Under these conditions, the primary mechanism for further cluster growth is Oswald ripening, which proceeds by the exchange of single vacancies between immobile clusters.

3.2 MD-regressed KMC model

In this model, the KMC vacancy–vacancy bond energies and the overall attempt frequency, ν_0, are determined by regression to the MD evolution data shown in figure 5. Both monomer (X_1) and dimer (X_2) numbers and several distribution moments (M_0, M_2, M_3, M_5 and M_7) are used in the regression to ensure that all cluster sizes contribute to the regressed KMC bond energies, while at the same time maintaining statistical quality in the MD data. An excellent representation of the MD dynamics is now shown in figure 5 for both the individual component and moment metrics.

Interestingly, the regressed value of the overall attempt frequency, ν_0, is such that the predicted single isolated

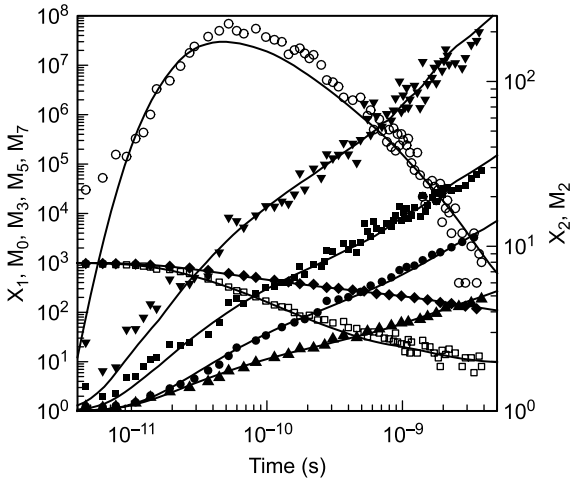

Figure 5. Comparison of MD and MD-regressed KMC model predictions for the vacancy cluster size evolution. Evolution profiles are symbols for MD, solid line for KMC: X_1—monomer (open squares); X_2—dimer (open circles); M_0—number of clusters (solid diamonds); M_2—average cluster size (solid circles); M_3—third-order moment (solid deltas); M_5—fifth-order moment (solid squares); M_7—seventh-order moment (solid gradients).

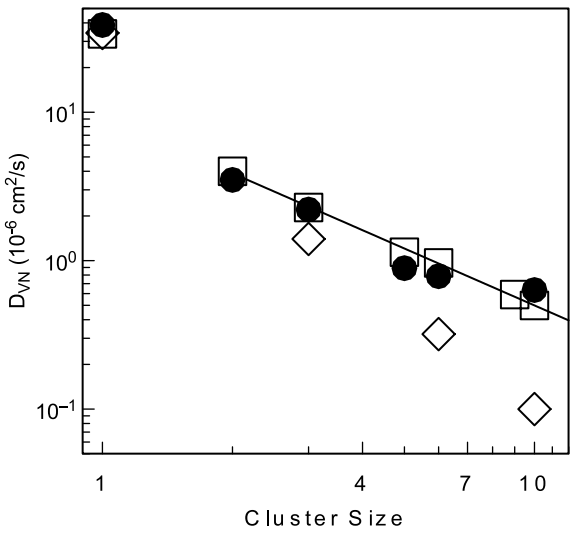

Figure 6. Comparison of cluster diffusivities predicted by: (a) MD-regressed KMC model (solid circles); (b) lattice-cluster KMC model (diamonds); and (c) MD (squares). Line is a power-law fit to the MD data for cluster size ≥ 2.

vacancy diffusivity, given by $D_{V1} = \mathrm{l}^2_{\mathrm{jump}}\nu_0 \exp(-\Delta E_{\mathrm{hop}}/k_BT)$ where l_{jump} is the jump length (1NN), is in excellent agreement with the MD value. This is not the case when the regression is repeated using KMC models with shorter ranged interactions. As the vacancy–vacancy interaction range is shortened, the predicted cluster structures become more compact and therefore less mobile and the regressed value of ν_0 increases to compensate, leading to an overestimate for the single vacancy diffusivity. In fact, even truncating the interaction at the 7th nearest-neighbor distance increases the regressed single vacancy diffusivity to about 25% above the MD value. At the shortest interaction range possible (nearest-neighbors) the regressed vacancy diffusivity is almost 250% larger than the MD value. Further discussion of this effect is provided in Ref. [24].

A comparison of the KMC predicted cluster diffusivities and the MD calculated values for several different cluster sizes is shown in figure 6. The MD-regressed KMC model is able to capture the correct cluster diffusion behavior, while the lattice-cluster model severely underpredicts the mobility of clusters. Note that in the latter case, the correct single vacancy diffusivity is ensured because ν_0 was fixed to reproduce it but in the former this agreement is a direct result of the regression process.

It is instructive also to consider the equilibrium cluster morphologies predicted by the two KMC models in relation to the MD structures. Shown in figure 7 are 35-vacancy cluster configurations following long equilibrations with the lattice-cluster and MD-regressed KMC models. In both cases, the initial configuration was taken to be the perfect octahedral structure, which is the energetic ground state. While the lattice-cluster model predicts a largely intact compact structure, the MD-regressed KMC model leads to a highly extended, loosely bound structure. As demonstrated above, the latter structure is much more mobile because it is able to reconfigure through a sequence of low energy barrier processes, which collectively lead to center-of-mass motion. Also shown in figure 7(c) is a structure predicted by direct EDIP MD simulation of a 35-vacancy cluster at 1600 K. In this case, it is somewhat difficult to identify the exact vacancy positions because of the extensive off-lattice nature of the atoms. The "vacancies" shown in figure 7(c) correspond to the 35 lattice sites that are furthest away from atom coordinates following energy minimization. Clearly, the MD-regressed KMC model cluster configurations are more consistent with the MD structure than the lattice-cluster KMC one. This comparison can be enhanced using an order-parameter to further characterize the structures of the clusters in figure 7. A structural parameter, defined as $r^n_{\mathrm{sep}} = \sqrt{\sum_i \sum_{j>i} (r_i - r_j)^2}$, was introduced to measure the total distance between vacancy pairs in each cluster. For the structures in figure 7(a–c), we obtained $r^{35}_{\mathrm{sep}} = 118$, 152 and 167 Å, further demonstrating the significant expansion associated with both the MD and MD-regressed KMC clusters, relative to the lattice-cluster KMC structure.

3.3 The impact of cluster configurational entropy

The large discrepancies in the cluster structures, diffusivities and aggregation dynamics predicted by the two KMC models can be explained on the basis of cluster configurational entropy. We have recently shown that the high temperature properties of atomic clusters in silicon

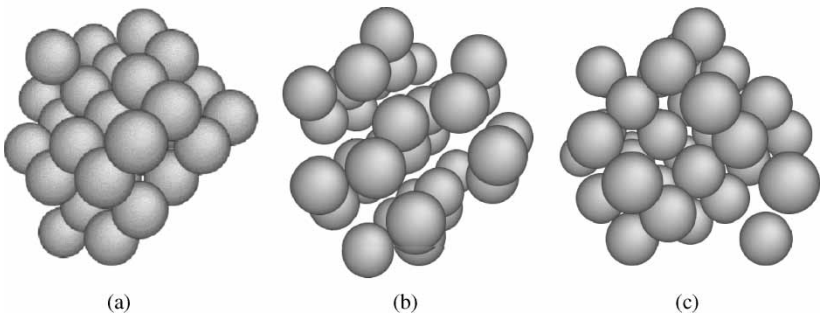

Figure 7. Comparison of cluster morphologies predicted by: (a) lattice-cluster model; (b) MD-regressed model; and (c) MD simulation.

Downloaded At: 18:13 14 January 2011

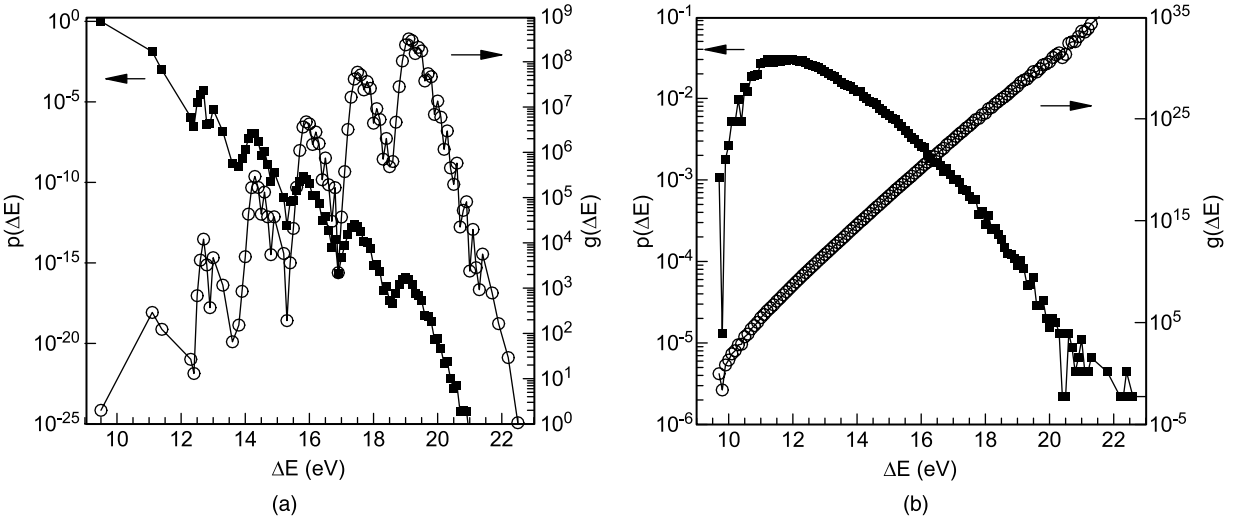

Figure 8. Density-of-states (DOS) (open symbols) and probability distribution functions (PDF) (filled symbols) for: (a) on-lattice; and (b) continuous space representations of the six-vacancy cluster.

Downloaded At: 18:13 14 January 2011

are dominated by the presence of an extremely large number of mechanically stable off-lattice configurations [28] that cannot be captured explicitly by a lattice model. This point is illustrated in figure 8(a) and (b), which show the equilibrium probability distribution (PDF) and the absolute density-of-states (DOS) functions for the formation energy of the six-vacancy cluster, calculated in two different ways. As defined here, the absolute DOS represents the number of distinct configurations that possess a given formation energy.

In figure 8(a), the DOS is computed using an on-lattice Wang–Landau Monte Carlo approach [30] which is described in detail in Ref. [28]. Briefly, a sequence of on-lattice configurations are generated and locally relaxed by energy minimization. Each configuration is generated by moving a single vacancy to another lattice site while retaining the cluster connectivity; i.e. only configurations corresponding to a bound cluster are considered. The Wang–Landau MC move acceptance criterion is based on the relative values of the DOS function before and after each proposed move. The formation energies of the visited configurations are histogrammed to create a converged DOS function, $g(\Delta E)$, from which the PDF, $p(\Delta E)$, can be computed as

$$p(\Delta E) = g(\Delta E)\exp(-\beta\Delta E)\exp\left(\frac{S_{\mathrm{vib}}(\Delta E)}{k_B}\right). \qquad (5)$$

The last term in equation (5) represents the contribution of the vibrational entropy to the PDF; more extended configurations tend to introduce additional vibrational states and therefore have higher vibrational entropy. Thus, the probability of finding the six-vacancy cluster in a configuration with formation energy ΔE at temperature T, depends on the Boltzmann weighted number of distinct configurations with that energy and the average vibrational entropy of configurations with that formation energy.

Two important points can be noted in figure 8(a). The first is that the DOS function attains a maximum value of almost 10^9 at $\Delta E = 19$ eV, demonstrating the large number of distinct configurations present even in the six-vacancy case. The second is that in spite of this large number, the PDF indicates that the most likely configuration is still the energetic ground state (at 9.6 eV). The energetic ground state for the six-vacancy cluster is a well-studied hexagonal ring-like structure [26,31] that has been shown to be extremely stable and in fact the entropic contribution due to both vibrational and (on-lattice) configurational degrees-of-freedom are not sufficient to alter the ground state even at temperatures close to the melting point.

In the second approach, the PDF was derived by evolving a system containing a six-vacancy cluster with EDIP MD at 1600 K and quenching the coordinates periodically to calculate the formation energy of the current configuration to create a histogram. The DOS was then computed from the PDF using equation (5). Clearly, the DOS for this case, shown in figure 8(b), indicates that the number of degenerate configurations present at each energy level is much higher than for the on-lattice case shown in figure 8(a). Moreover, there is now a much higher density of possible energy levels. The total number of configurations now available leads to a very large configurational entropic contribution to the total free energy and shifts the maximum in the PDF to some intermediate value (about 11.8 eV) which corresponds to extended, disordered cluster structures of the type shown in figure 7(b) and (c). The source of these additional configurations is the large number of possible significant lattice rearrangements around a vacancy cluster, which cannot be captured by static relaxation in the neighborhood of an on-lattice configuration. In other words, the potential energy surface around a vacancy cluster is extremely rugged and consists of numerous distinct local minima. Additional details regarding this aspect can be found in Ref. [28].

The DOS and PDF functions in figure 8 provide an explanation for the failure of the lattice-cluster KMC model.

Downloaded At: 18:13 14 January 2011

High temperature clusters are strongly influenced by the presence of a large number of off-lattice mechanically stable configurations. Thus, any rate database constructed on the basis of transitions between on-lattice configurations will not provide an accurate picture. The MD-regression KMC model, while still an on-lattice representation, accounts for the correct thermodynamics through effective bond "free energies" that implicitly include the entropic contributions from the off-lattice configurations. In some sense, each cluster in this model is a representative structure for many neighboring distinct off-lattice configurations. In the same vein, the KMC bonding model embodied in equation (2), along with the regressed bond "free energies" can be regarded as a "lattice-potential" for vacancy clusters in silicon that correctly captures the entropic contribution of the missing degrees-of-freedom. Unfortunately, because of the implicit temperature dependence of the PDF in figure 8(b), the lattice potential is only valid at the regression temperature, 1600 K. In previous continuum modeling work, we have shown that these entropic effects and their resulting impact on high-temperature vacancy cluster properties have profound impacts on the predicted cluster size distribution, leading to much better agreement with experimental measurements in commercial silicon wafers [18].

3.4 Improving the database for MD-regressed KMC models

The MD evolution data shown in figures 4 and 5 are limited to very small timescales (several ns) and atomic processes that occur on slower timescales are not transmitted to the KMC rate parameters. The high temperature used in the present work mitigates some of these limitations for the specific case of vacancy aggregation but increasing the scope of the data that is used to parameterize the KMC model should generally increase the chances for a robust description. Moreover, the data contained in figures 4 and 5 is highly non-equilibrium in nature because of the high degree of supersaturation needed to achieve aggregation within the short MD timescale.

To better understand how the MD database used to regress the KMC parameters can be improved it is instructive to consider a mean-field description of a generic aggregation process, which can be described by a series of aggregation and fragmentation processes, i.e.

$$X_i + X_j \underset{B(i,j)}{\overset{F(i,j)}{\leftrightarrow}} X_{i+j} + X_l \underset{B(i+j,l)}{\overset{F(i+j,l)}{\leftrightarrow}} X_{i+j+l}, \tag{6}$$

where

$$\frac{\mathrm{d}X_k}{\mathrm{d}t} = \frac{1}{2}\sum_{i+j=k}\left[F(i,j)X_iX_j - B(i,j)X_{i+j}\right] - \sum_{l=1}^{\infty}\left[F(k,l)X_kX_l - B(k,l)X_{k+l}\right]. \tag{7}$$

In equation (7), the forward, $F(i,j)$ and backward, $B(i,j)$, kernels are given by

$$F(i,j) \sim (D_i + D_j) \times \left(r_i^{\mathrm{cap}} + r_j^{\mathrm{cap}}\right)^2 \exp\left(-\frac{\Delta G_{i+j\rightarrow(i+j)}}{k_BT}\right), \tag{8}$$

and

$$B(i,j) = \frac{F(i,j)\cdot X_i^{\mathrm{eq}}\cdot X_j^{\mathrm{eq}}}{X_{i+j}^{\mathrm{eq}}}. \tag{9}$$

The preceding expressions indicate that an aggregation process is generally a function of three key ingredients: (1) cluster diffusivities; (2) cluster structures; and (3) cluster equilibrium concentrations (for dissolution). The highly non-equilibrium process used to parameterize the KMC model in figure 5 is strongly driven in the forward direction and therefore depends only weakly on the cluster equilibrium concentrations. However, it is strongly dependent on the cluster effective sizes and diffusivities. As shown previously in figure 6, the cluster diffusivities are indeed captured accurately by the regression process. The question we now address is whether the other properties are captured in any meaningful manner.

A more detailed analysis of the predicted cluster structures is presented in figure 9, which shows a comparison of the vacancy density distributions in a 35-vacancy cluster predicted by the MD-regressed KMC model and MD simulation. The density distribution, $\rho(r)$, is defined as the number of vacancies per shell divided by the volume of the shell, averaged over many cluster configurations. The distributions shown in figure 9 are binned into intervals of width 0.1 of the nearest-neighbor distance. Notably, the density profiles match closely in the region of the tail ($r/\sigma \geq 2$). This agreement is expected because the density distribution in this region sets the overall capture volume of the cluster. However, the density profile in

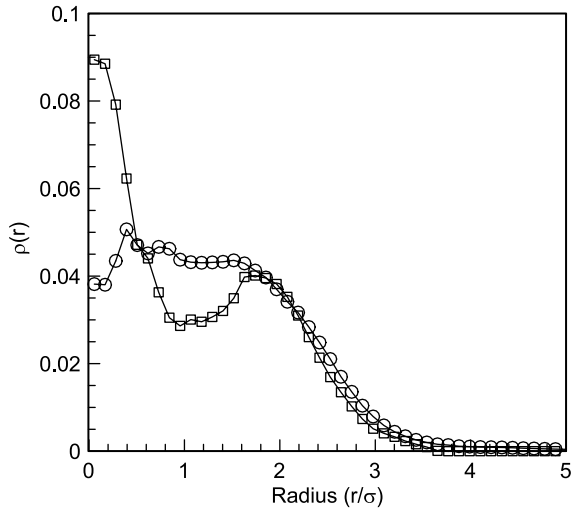

Figure 9. Averaged vacancy density profiles for a 35-vacancy cluster: (a) MD simulation (squares); (b) MD-regressed KMC simulation (circles). $\sigma = 2.0951$ Å is the interatomic potential length scale.

the cluster interior is qualitatively poor. While the MD cluster is characterized by a dense core surrounded by a diffuse halo, the KMC cluster density is almost evenly distributed throughout the radius of the cluster. This discrepancy arises because the MD evolution data provides information on the effective cluster size and not on the internal structure of cluster. Static relaxation (energy minimization) shows that the MD structures are much lower in energy than the KMC ones even though they have comparable capture volumes. It is therefore reasonable to expect that including data of the type shown in figure 9 into the database could further refine the overall accuracy of the KMC model.

Finally, it should also be noted that in the present case, all clusters are approximately spherical and the issue of cluster internal density distribution is not important for predicting the correct dynamics. In fact, it is not clear whether a one-to-one correspondence is meaningful given that, as mentioned earlier, each on-lattice cluster configuration in the present model is a representative structure for an ensemble of off-lattice structures. On the other hand, it is expected that in cases where the cluster shapes and capture zones are not spherical, structural information would be required in the MD database. This issue will be addressed in future work.

The thermodynamic properties of the clusters predicted by the MD-regressed KMC model were probed using a sequence of runs in which 50 vacancies were allowed to approach equilibrium in systems of various sizes ranging from 13,824 to 46,656,000 sites. The KMC equilibrium cluster size distributions for 20 KMC systems each with 50 vacancies are shown in figure 10. The equilibrium distributions in each system were obtained by monitoring the size distribution until system equilibration and then collecting up to 50,000 distribution samples for averaging. The sample interval was 2000 vacancy hops. The transition from a clustered configuration to an unclustered one can be clearly seen at a system size of about 3×10^5.

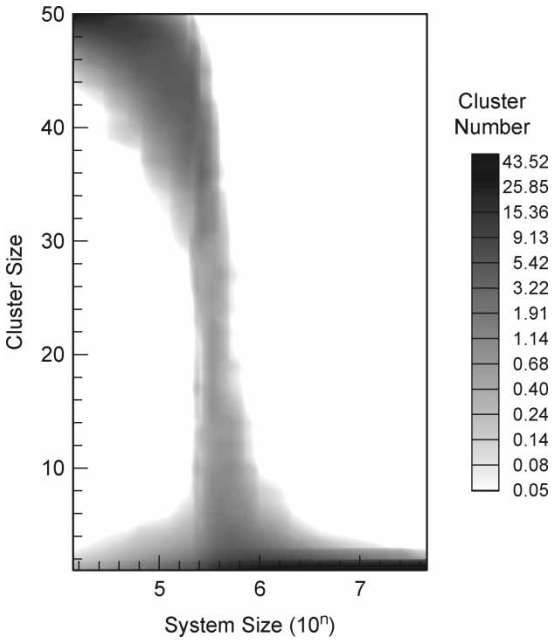

Figure 10. The equilibrium cluster size distribution for 50 vacancies as a function of system size from MD-regressed KMC simulations.

The total free energy of a closed lattice containing a fixed number of vacancies, N_{tot}, is given by

$$G = G_0 + \sum_i^{N_{\max}} X_i \Delta G_i - k_B T \sum_i^{N_{\max}} \left\{ X_i \ln i + \frac{N_s}{i} \ln\left(\frac{N_s}{i}\right) - \left[\frac{N_s}{i} - X_i\right] \ln\left[\frac{N_s}{i} - X_i\right] - X_i \ln X_i \right\}, \tag{10}$$

subject to the constraint that

$$\sum_i^{N_{\max}} i X_i = N_{\text{tot}}, \tag{11}$$

where G_0 is a reference free energy, defined here as the free energy of a perfect lattice with the same total number of lattice sites, N_s. X_i is the number of clusters containing i vacancies and $N_{\max}(= N_{\text{tot}})$ is the maximum possible cluster size. Equation (11) is the vacancy conservation statement for the closed system. The second term on the left-hand side of equation (10) represents the total internal free energy of formation for all clusters in the system, which includes enthalpy and internal cluster vibrational and configurational entropy, i.e.

$$\Delta G_i = \langle \Delta E_i \rangle - T \langle \Delta S_{i,\text{vib}} \rangle - T S_{i,\text{conf}}. \tag{12}$$

In equation (12), the angular brackets reflect the fact that each cluster can assume an ensemble of configurations as discussed in the previous section. The last summation in equation (10) gives the translational entropy of the system and reflects the number of ways that an ensemble of clusters of different sizes can be arranged within the lattice. It is important to distinguish the translational entropy from the internal configurational entropy of each cluster; the latter reflects the number of configurations that a cluster can attain *per lattice site*.

At equilibrium, the total free energy of the system is minimized subject to the constraint that the total number of vacancies is fixed. Generally, the cluster free energies of formation are known and the equilibrium concentrations can be determined based on this condition. In the present case, the equilibrium distribution is known and the cluster free energies are the unknowns. An optimization problem can be formulated by defining an augmented free energy function as

$$\hat{G} = G_0 + \sum_i^{N_{\max}} X_i \Delta G_i - k_B T \sum_i^{N_{\max}} \left\{ X_i \ln i + \frac{N_s}{i} \ln\left(\frac{N_s}{i}\right) - \left[\frac{N_s}{i} - X_i\right] \ln\left[\frac{N_s}{i} - X_i\right] - X_i \ln X_i \right\} + \lambda \left(\sum_i^{N_{\max}} i X_i - N_{\text{tot}} \right), \tag{13}$$

Downloaded At: 18:13 14 January 2011

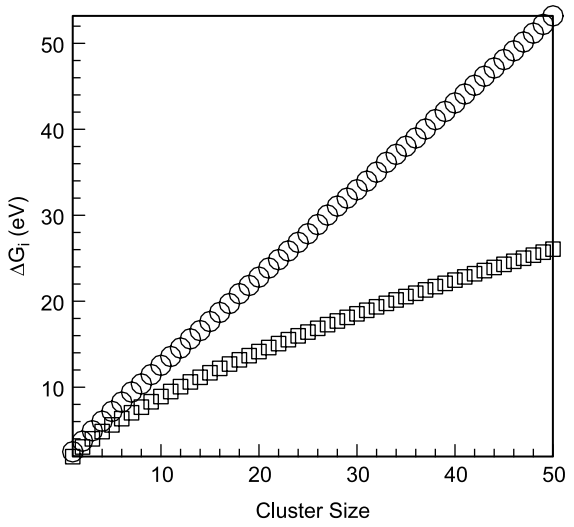

Figure 11. Comparison of cluster free energies of formation from MD-regressed KMC simulations (circles) and MD data (squares).

where the last term represents the vacancy number constraint and λ is a Lagrange multiplier. At equilibrium, the derivatives of the augmented free energy with respect to the number of each cluster size are equal to zero and are given by

$$\frac{\partial \hat{G}}{\partial X_i} = \Delta G_i - k_B T \ln \frac{N_s - iX_i}{X_i} + i\lambda = 0,$$
$$i = 1,2,\ldots,N_{\max}. \tag{14}$$

This is equivalent to the statement that for each possible reaction in the system, e.g. $V_1 + V_1 \rightarrow V_2$ or $V_1 + V_2 \rightarrow V_3$, $\sum_i \nu_i \mu_i = 0$ where $\mu = \partial G/\partial X_i$ is the chemical potential and ν_i are the stoichiometric coefficients. The set of equations in equation (14) provide relationships between system size, cluster size distribution and cluster formation free energies. Note that $\partial \hat{G}/\partial \lambda = 0$ simply returns the constraint and is automatically satisfied by the KMC distribution data.

The cluster free energies of formation were computed using equation (14) and the data in figure 10 for all system sizes. The cluster free energies of formation are shown in figure 11 and appear to scale linearly with cluster size, although slight deviations are present for very small clusters. Also shown in figure 11 are the free energies of formation as computed by MD in previous work, which scale as $n^{2/3}$. The difference in the scaling behavior highlights the fact that the thermodynamic picture captured by the KMC model is not correct. Once again, this is not unexpected because very little thermodynamic information was present in the strongly non-equilibrium MD data shown in figures 4 and 5. Practically, this implies that a near-equilibrium KMC simulation using the current model would not provide accurate results. It remains to be seen whether the existing bond-counting model can simultaneously capture the correct cluster microstructure, thermodynamics and diffusivities; this will be addressed in future work which will be aimed at designing optimal MD databases for regressing KMC models.

4. Conclusions

A bond-counting on-lattice KMC model for vacancy diffusion and aggregation in silicon at elevated temperature was generated by regression to MD-generated data. In the present study, the MD database was built using a single large-scale non-equilibrium simulation in which 1000 vacancies were allowed to diffuse and cluster in a 216,000-lattice site system at 1600 K and zero pressure for about 4 ns. Various measures of the transient cluster size distribution were used to tune the KMC model.

The MD-regressed KMC model was shown to provide an excellent representation of vacancy clustering dynamics. The model was analyzed by comparing the predicted cluster diffusivities, structures and thermodynamics to values computed by independent MD simulations. Both cluster diffusivities and effective capture volumes were captured well by the KMC model even though these were not explicitly considered during the regression. On the other hand, the microscopic distribution of vacancies within the cluster interiors and the cluster thermodynamic properties were not well captured by the KMC model because the non-equilibrium MD simulation data used in this study is not sensitive to them. Note that the formation thermodynamics of clusters as a function of size is only important for equilibrium and near-equilibrium simulations. Future work will be aimed at expanding the MD database used to tune the KMC model parameters to determine whether a more direct connection between KMC and MD can be made.

This investigation also highlighted a general difficulty encountered in performing lattice KMC simulations at elevated temperature. At higher temperatures, atomic clusters in crystals are strongly influenced by off-lattice configurations that cannot be explicitly captured in lattice models. The present work provides an avenue for coarse-graining these configurations onto a lattice framework in a way that captures the effect of configurational entropy, while retaining the computational advantages of a lattice-based method.

Acknowledgements

We gratefully acknowledge financial support from the National Science Foundation (CTS01-34418) and the Department of Chemical and Biomolecular Engineering at the University of Pennsylvania.

References

[1] A.F. Voter. Classically exact overlayer dynamics: diffusion of rhodium clusters on Rh(100). *Phys. Rev. B*, **34**, 6819 (1986).

Downloaded At: 18:13 14 January 2011

[2] E.S. Hood, B.H. Toby, W.H. Weinberg. Precursor-mediated molecular chemisorption and thermal desorption: The interrelationships among energetics, kinetics, and adsorbate lattice structure. *Phys. Rev. Lett.*, **55**, 2437 (1985).
[3] M.E. Law, G.H. Gilmer, M. Jaraiz. Simulation of defects and diffusion phenomena in Silicon. *MRS Bull.*, **25**, 45 (2000).
[4] J.B. Adams, Z.Y. Wang, Y.H. Li. Modeling Cu thin film growth. *Thin Solid Films*, **365**, 201 (2000).
[5] R. Pinacho, P. Castrillo, M. Jaraiz, I. Martin-Bragado, J. Barbolla, H.-J. Gossmann, G.H. Gilmer, J.L. Benton. Carbon in Silicon: Modeling of diffusion and clustering mechanisms. *J. Appl. Phys.*, **92**, 1582 (2002).
[6] O. Biham, I. Furman, M. Karimi, G. Vidali, R. Kennett, H. Zeng. Models for diffusion and island growth in metal monolayers. *Surf. Sci.*, **400**, 29 (1998).
[7] L.G. Wang, P. Clancy. Kinetic Monte Carlo simulation of the growth of polycrystalline Cu films. *Surf. Sci.*, **473**, 25 (2001).
[8] O. Trushin, A. Karim, A. Kara, T.S. Rahman. Self-learning kinetic Monte Carlo method: Application to Cu(111). *Phys. Rev. B*, **72**, 115401 (2005).
[9] H. Eyring. The activated complex in chemical reactions. *J. Chem. Phys.*, **3**, 107 (1935).
[10] A.F. Voter, J.D. Doll Transition state theory description of surface self-diffusion: Comparison with classical trajectory results. *J. Chem. Phys.*, **80**, 5832 (1984).
[11] G.H. Vineyard. Frequency factors and isotope effects in solid state rate processes. *J. Phys. Chem. Solids*, **3**, 121 (1957).
[12] P. Hanggi, P. Talkner, M. Borkovec. Reaction-rate theory: fifty years after Kramers. *Rev. Mod. Phys.*, **62**, 251 (1990).
[13] K.A. Fichthorn, M.L. Merrick, M. Scheffler. A kinetic Monte Carlo investigation of island nucleation and growth in thin-film epitaxy in the presence of substrate-mediated interactions. *Appl. Phys. A*, **75**, 17 (2002).
[14] M. Itsumi, H. Akiya, T. Ueki, M. Tomita, M. Yamawaki. The composition of octahedron structures that act as an origin of defects in thermal SiO_2 on Czochralski silicon. *J. Appl. Phys.*, **78**, 5984 (1995).
[15] E. Dornberger. Prediction of OSF ring dynamics and growth-in voids in Czochralski Silicon crystals. PhD Thesis, Universite Catholique de Louvain, Belgium (1998).
[16] T. Sinno, R.A. Brown. Modeling microdefect formation in Czochralski Silicon. *J. Electrochem. Soc.*, **146**, 2300 (1999).
[17] M. Prasad, T. Sinno. Internally consistent approach for modeling solid-state aggregation. II. Mean-field representation of atomistic processes. *Phys. Rev. B*, **68**, 045207 (2003).
[18] T. Frewen, M. Prasad, W. Haeckl, W. von Ammon, T. Sinno. Microscopically accurate continuum model for void formation during semiconductor Silicon processing. *J. Cryst. Growth*, **279**, 258 (2005).
[19] M.Z. Bazant, E. Kaxiras, J.F. Justo. Environment-dependent interatomic potential for bulk Silicon. *Phys. Rev. B*, **56**, 8542 (1997).
[20] J. Tersoff. New empirical approach for the structure and energy of covalent systems. *Phys. Rev. B*, **37**, 6991 (1988).
[21] F. Stillinger, T.A. Weber. Computer simulation of local order in condensed phases of Silicon. *Phys. Rev. B*, **31**, 5262 (1985).
[22] A. Bongiorno, L. Colombo. Interaction between a mono-vacancy and a vacancy cluster in Silicon. *Phys. Rev. B*, **57**, 8767 (1998).
[23] M. Prasad, T. Sinno. Internally consistent approach for modeling solid-state aggregation. I. Atomistic calculations of vacancy clustering in silicon. *Phys. Rev. B*, **68**, 045206 (2003).
[24] J. Dai, J.M. Kanter, S.S. Kapur, W.D. Seider, T. Sinno. On-lattice kinetic Monte Carlo simulations of point defect aggregation in entropically influenced crystalline systems. *Phys. Rev. B*, **72**, 134102 (2005).
[25] A. La Magna, S. Coffa, L. Colombo. A lattice kinetic Monte Carlo code for the description of vacancy diffusion and self-organization in Si. *Nucl. Instrum. Methods. Phys. Res. B*, **148**, 262 (1999).
[26] M. Prasad, T. Sinno. Atomistic-to-continuum description of vacancy cluster properties in crystalline Silicon. *Appl. Phys. Lett.*, **80**, 1951 (2002).
[27] K.A. Fichthorn, M. Scheffler. Island nucleation in thin-film epitaxy: A first-principles investigation. *Phys. Rev. Lett.*, **84**, 5371 (2000).
[28] S.S. Kapur, M. Prasad, J.C. Crocker, T. Sinno. Role of configurational entropy in the thermodynamics of clusters of point defects in crystalline solids. *Phys. Rev. B*, **72**, 014119 (2005).
[29] M.P. Allen, D.J. Tildesley. *Computer Simulation of Liquids*, Oxford University Press, Oxford (1987).
[30] F. Wang, D.P. Landau. Efficient, multiple-range random walk algorithm to calculate the density of states. *Phys. Rev. Lett.*, **86**, 2050 (2001).
[31] A. Bongiorno, L. Colombo, T. Diaz De la Rubia. Structural and binding properties of vacancy clusters in Silicon. *Europhys. Lett.*, **43**, 695 (1998).

Downloaded At: 18:13 14 January 2011